



Temperature and Stress Evaluation during Friction Stir Welding of Inconel 718 Alloy Using Finite Element Numerical Simulation

Ranamay Saha and Pankaj Biswas

Submitted: 3 August 2021 / Revised: 7 September 2021 / Accepted: 25 September 2021 / Published online: 12 October 2021

The current work aims to carry out a dynamic explicit nonlinear finite element simulation to analyze the temperature and residual stress distribution during friction stir welding process of Inconel 718 alloy. The computational modeling has been done in the ABAQUS[®] explicit software. Features such as arbitrary Lagrangian-Eulerian formulation, adaptive meshing, mesh sensitivity analysis and mass scaling have been incorporated in order to develop a reliable and computationally efficient FE model. A finite sliding property was used to define the interaction between tool bottom surface and plate upper surface. The tool-workpiece contact was defined with coulomb friction model with temperature-dependent friction coefficient value. Furthermore, a small experimental work was carried out in order to validate the numerically obtained thermal profiles. Results showed that similar temperature profiles were generated across the workpiece. However, temperatures in advancing side were slightly on a higher side. Mechanical response of the Inconel plates was also studied.

Keywords finite element model, friction, FSW, inconel 718 alloy, stress, temperature

1. Introduction

Friction stir welding (FSW) is a solid-state joining process which has gained immense popularity since its introduction in 1991 because of its great potential to join difficult-to-weld metallic materials such as aluminum and magnesium alloys (Ref 1). Research on FSW primarily focused on light alloys over the past decades. However, currently the process capability has been extended to various other metals and alloys such as copper and its alloys, titanium and its alloys, lead, nickel, zinc, stainless steel and mild steel, dissimilar alloys and metal matrix composites (Ref 2). Despite major advances in the application of FSW to multiple metallic materials, the fundamental knowledge of the complex thermal and thermomechanical processes involved is still not completely understood (Ref 3). FSW involves various sophisticated process mechanisms which are hard to visualize and analyze through experimental investigations. In recent years, serious effort is being done toward understanding the mechanisms and physical processes involved in the various stages of FSW process (Ref 4) and numerical simulations are an integral part of that. The investigations by Yu et al. on 7050 aluminum alloy plates showed that the temperature distribution was quite symmetrical across the plate width with a ‘V’ pattern contour in the nugget zone. The dwell stage involved generation of the frictional heat to preheat the plate. The traverse stage was characterized by

heat generation until a quasi-stable temperature field was formed. Also, it was observed that the thermal profiles varied significantly with the variation of heat conduction through the back plate. Pankaj et al. performed a heat transfer analysis through a FE model developed in ABAQUS software to study the effect of traverse speed on the thermal history during FSW of low carbon steel (Ref 6). Results obtained were in good correlation to the experimental work. Chen and Kovacevic also performed a similar work to study the thermal and coupled mechanical response of the workpieces during FSW process. The physical tool and shoulder were represented as a moving heat generation at the nodes during each time step by assigning a constant heat value accounting for frictional and plastic effect. However, despite yielding good results with thermal history, such models provide limited flexibility toward realistic results due to the negligence of tool profiles (Ref 3). Assidi et al. (Ref 9) used an arbitrary Lagrangian-Eulerian (ALE) technique to predict the forces and tool temperatures during FSW of Al 6061 aluminum plate. Coulomb’s law of friction and Norton’s frictional model were compared to find out the best model that suit numerical FSW formulations with respect to sensitivity and accuracy. Jain et al. developed a Lagrangian incremental model to predict the forces, torques, temperature and equivalent plastic strain for friction stir butt welding of AA2024-T4 plates. Results were validated with experimental findings. Force and torque reduced with increase in tool rotational speed (Ref 10). Chao et al. (Ref 11) have performed heat transfer simulations for steady-state and transient boundary value problem. Temperature-coupled stress evolutions on the weld samples were also studied. However, they neglected the plastic heat generation. Al-Badour et al. (Ref 16) implemented the coupled Eulerian-Lagrangian (CEL) algorithm in ABAQUS environment to investigate FSW of dissimilar Al6061-T6 and Al5083-O aluminum alloys. The FSW tool was treated as a Lagrangian body, while the workpiece was defined as an Eulerian body. Investigation on void formation revealed close correlation with friction coefficients. Salloomi et al. developed a finite element

Ranamay Saha and Pankaj Biswas, Department of Mechanical Engineering, Indian Institute of Technology Guwahati, Guwahati, Assam 781039, India. Contact e-mail: ranamaysaha@gmail.com.

(FE) model to carry out explicit thermomechanical analysis of the three different stages (plunge, dwell and traverse) of FSW process. A detailed analysis revealed symmetrical temperature distribution across the plate width and that temperature plays a significant role toward stress evolution on the AA 7075-T651 alloy plates. The advancing side (AS) showed a higher plastic strain value than the retreating side (RS) (Ref 7). There is a similar study on AZ91 magnesium alloys plates to understand the nature of distribution of residual stresses along with the thermal history (Ref 5). Riahi and Nazari (Ref 17) developed a FE simulation model to study the temperature distribution and consequent residual stresses in friction stir welding of aluminum alloy 6061-T6. Numerical results were in correlated well to the experimental results. However, their work did not consider the pin of the FSW tool. A coupled thermomechanical finite element model in ABAQUS actuated by a Fortran program was used by Zhang et al. [8] to study the FSW process of AA2024-T3 for different plate thicknesses. Material flow was higher on the retreating side, and heat fluxes were higher on the advancing side. Also, plastic strain decreased in the thick plates. Zhang et al. concluded that weaker stirring action led to lower strain in the thick plates and that FSW was more effective in welding thin plates. Mandal et al. (Ref 13) specifically focused on the study of thermomechanical analysis of the plunge stage. It is to be noted that a lot of research ignore the plunge stage during numerical study of FSW due to the occurrence of heavy mesh distortions and early model terminations (Ref 12, 14). However, consideration of all the stages is very important to formulate a good numerical model.

The present study aims to implement an arbitrary Lagrangian-Eulerian (ALE) formulation to perform an explicit fully coupled thermomechanical analysis of friction stir welding process. The material under consideration is Inconel 718 alloy. Strain rate and temperature-dependent Johnson-Cook material model for Inconel 718 alloy (Ref 15) is incorporated in the FE analysis. The current FE model can compute temperature, stresses and strains at various time intervals during the FSW process namely plunge, dwell and traverse stage. Finite sliding property was used to define the interaction between tool bottom surface and plate upper surface. Moreover, an experimental work is also done to validate the numerically obtained results through comparison of the recorded thermal history using k-type thermocouples. The numerical results correlate well with the experimental results observed in this work as well as to experimental results found in the literature.

2. Experimental Work

2.1 Setup Developed for FSW

A suitable fixture was designed to hold the workpiece during the friction stir welding of Inconel 718 plates as shown in Fig. 1. Fixture was developed in order to hold the workpiece during welding and to measure the temperature during the welding. Workpieces were clamped rigidly at the bottom and all sides to avoid shaking and vibrations due to the high forces generated during the welding processes. Inconel 718 alloy was selected as the workpiece material. Rolled plates of 3 mm thickness were cut into the required size (210 mm × 80 mm × 3 mm) by shearing machine. The cut samples were faced in a

milling machine on both sides of the plates. After that burr was removed from the edges and the samples were then cleaned with acetone to eliminate any surface impurities. Welding was performed in the rolling direction in the butt joint configuration. Process parameters were fixed at a tool rotation speed of 300 rpm and traverse speed of 90 mm/min. FSW tool was made up of tungsten carbide (WC-10%Co) with AW25 grad, which was a flat shoulder diameter of 25 mm with a pin height of 2.7 mm. A constant axial load of 40 kN was applied on the tool.

2.2 Temperature Measurement

The transient temperature of the sample during friction stir welding was measured with K-type thermocouples. Two K-type thermocouples were used to trace the temperature time history of two points located at a distance of 15 mm from the weld line and 20 mm the bottom edge of the plate (Fig. 2). Thermocouple location was decided such that the thermomechanically affected zone (TMAZ) is avoided. This was to bar the displacement of the thermocouples by the stirring action of the tool.

Thermocouples are attached to a DAQ system that can sample the temperature data at 60 Hz and display them on a computer with a specialized program running on LabView software.

3. Model Description

The computational modeling of FSW of Inconel 718 has been done in the ABAQUS[®] explicit software. Arbitrary Lagrangian-Eulerian (ALE) approach was used with the adaptive mesh technology. Considering the Inconel plates as an adaptive mesh region with constraints and controls allows the mesh to move independent of the material motion. Therefore, a high-quality mesh is maintained even during large deformations and distortions. Mass scaling technique was used to bring down the computational time of simulation. Finite element method has been applied to simulate the thermomechanical behavior of friction stir welding of Inconel plates using WC-Co tool.

3.1 Computational Model

The present model is composed of the deformable plates made of Inconel 718 and a rigid tool. The actual plate dimensions were reduced to 100 mm × 50 mm × 3 mm to reduce computational time.

The rigid tool is made of tungsten carbide with 10 % cobalt. The model dimensions are shown in Fig. 3. The tool shoulder has a flat bottom with 25 mm diameter, and the pin is of conical shape with a height of 2.7 mm. The final part dimensions of the tool are considered same as that of the actual tool dimensions used in experiment. Eight-node coupled temperature displacement and brick elements with reduced integration (C3D8RT) were used to mesh the plates. Such elements have the ability to compute temperature and displacement in x, y and z directions in a dynamic explicit analysis. Mesh sensitivity analysis was done by experimenting with different meshing techniques such as structured meshing, variable meshing with partitioning and different mesh sizes. However, convergence occurred at a mesh size of 1 mm giving a balance between accuracy and computational speed. Figure 4 and 5 shows the final mesh. A total of 15000 linear hexahedral elements of type C3D8RT was generated in each of the Inconel 718 plates. And on the tool,

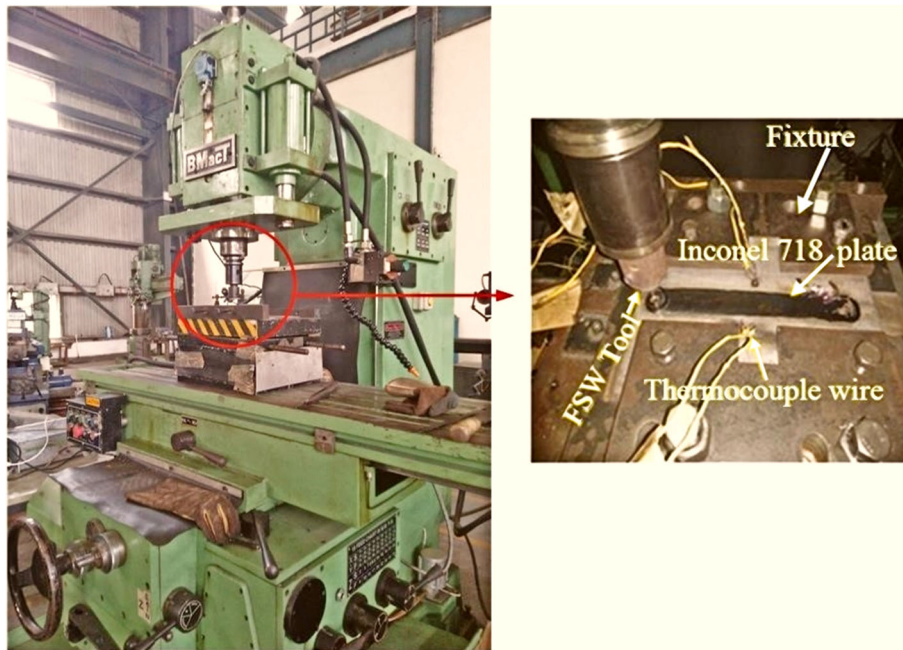


Fig. 1 Experimental setup of friction stir welding

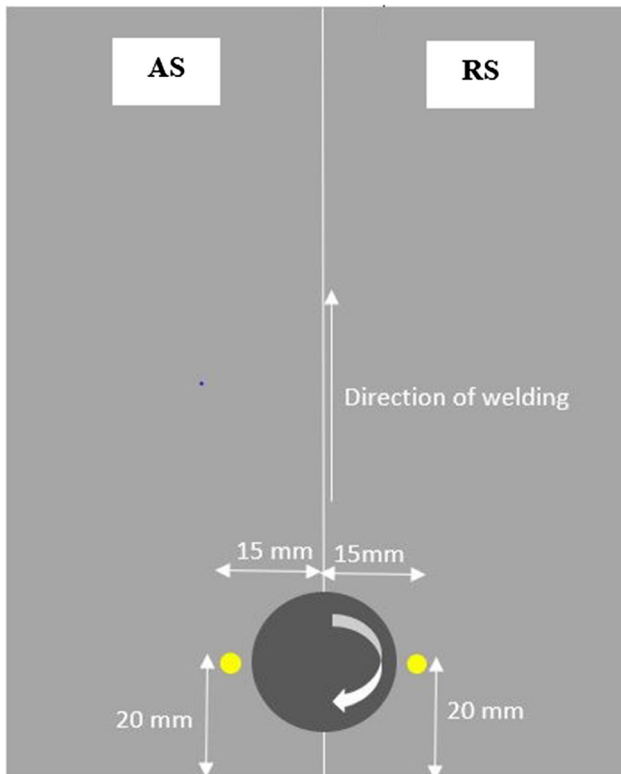


Fig. 2 Position of K-type thermocouples

65104 linear tetrahedral elements of type C3D4T was generated. Each element in this FEA model has both thermal and mechanical degree of freedom. The simulation was performed on a computer having specifications 7-core processor and 8 GB of RAM. This model can well be utilized to simulate friction stir welding in other situations such as with a different tool geometry or design. A different tool geometry can either be

modeled in ABAQUS part module or imported from any modeling software such as Solidworks or Catia. Plate thickness can be varied as per the design requirements of the user. Furthermore, parameter variations can also be carried out in order to optimize the working parameters ahead of actual experiment.

3.2 Material Model

The Johnson-Cook material model is used to define the plastic behavior as a function of strain hardening, strain rate hardening and thermal softening as given by the equation below:

$$(A + B\varepsilon^n) \left[1 + C \ln \left(1 + \frac{\dot{\varepsilon}}{\dot{\varepsilon}_o} \right) \right] \left[1 - \left(\frac{T - T_{\text{room}}}{T_{\text{melt}} - T_{\text{room}}} \right)^m \right] \quad (\text{Eq 1})$$

where ε and $\dot{\varepsilon}_o$ are plastic strain and strain rate, respectively. T is the melting point temperature, T_{room} is the ambient temperature. A , B , m , n , C , $\dot{\varepsilon}_o$ are the constants dependent on the material. The values adopted for these constants for Inconel 718 alloy are given in Table 1.

The melting point temperature is taken as 1320 °C and ambient temperature as 25 °C. The other mechanical and thermal properties used in the analysis are listed in Table 2.

3.3 Boundary Conditions

The heat source considered in this model is the frictional heat developed due to interaction between the tool and the plates. As friction coefficient depends heavily upon many factors like temperature, pressure and slip velocity, a temperature-dependent Coulomb friction coefficient has been chosen as shown in Table 3. A finite sliding property was used to define the interaction between tool bottom surface and plate upper surface. This notion helps the mesh to keep track of the material flow during the process.

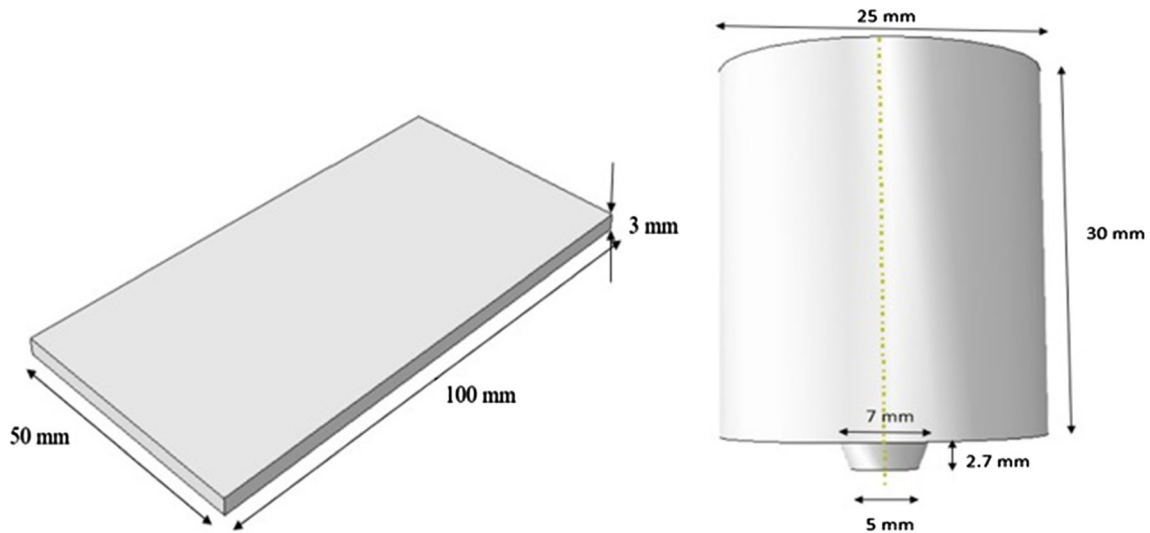


Fig. 3 Plate and tool dimensions as used in the FE model analysis

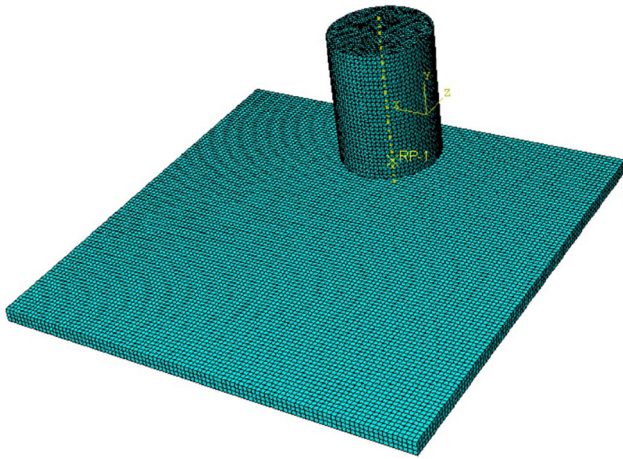


Fig. 4 The model assembly showing meshed plates

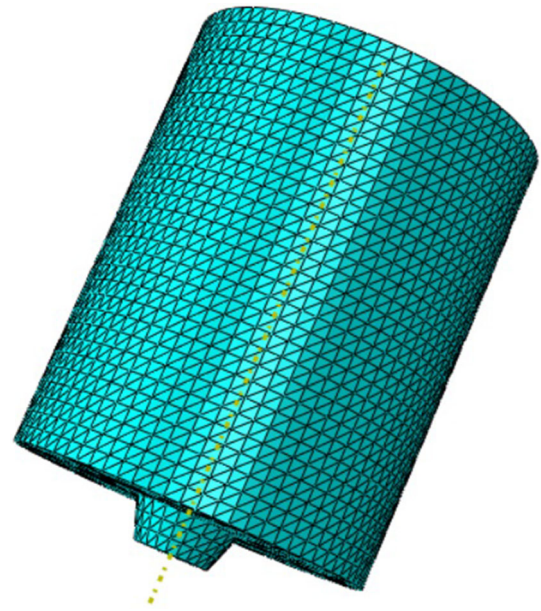


Fig. 5 Tet-meshed tool model

During the FSW of hard metals and alloys such as steels, considerably higher thermal conductivity of tungsten leads to the transfer of a significant amount of heat to the tool (Ref 6). In most of the earlier works in this direction, the energy dissipation value was chosen between 40 and 50% (Ref 21-23). Also, as Inconel alloys have conductivity values close to those of steels, the energy dissipation value in the current work has been decided to be in the range of 45-50% and has been validated by comparison of the numerical results with the temperature distribution curves obtained experimentally. The corresponding error between the experimental and numerical thermal profiles was found to be minimum when the dissipated energy value was chosen to be 50% of the total generated heat. Therefore, it is assumed that 100% of the frictional energy is converted to heat and 50% of the total frictional heat generated is dissipated into the plate. Furthermore, all the sides and top surface is exposed to ambient conditions.

The plates are fixed in all directions at the sides and bottom using encastre method (Fig. 6). A constant axial load of 40 kN is applied on the tool in vertical direction. Heat transfer through convection is defined by a factor of $30 \text{ Wm}^{-2} \text{ k}^{-1}$ for the top surface and the sides. As the bottom surface may be attached to

Table 1 Johnson-Cook parameters for Inconel 718 from the literature (Ref 15)

A, MPa	B, MPa	C	m	n	$\dot{\epsilon}$
450	1700	0.017	1.30	0.65	1.001

a backing plate in experimental conditions, complexity of contact gap conductance is taken care of by using a convective heat transfer coefficient of $500 \text{ Wm}^{-2} \text{ k}^{-1}$. It is to be noted that the FSW process contains three different phases. First is plunging step when the tool plunges up to a certain depth into the workpiece. Second is the dwell step which is considered just to rise the temperature of the workpiece for welding. And the last step is the traverse step in which the tool moves along

Table 2 Temperature-dependent material properties of Inconel 718 (Ref 20)

Temperature, °C	Density, kg m ⁻³	Specific heat, J kg ⁻¹ °C ⁻¹	Thermal conductivity, W m ⁻¹ °C ⁻¹
25	8190	435	107
100	8160	455	129
200	8118	479	154
300	8079	497	171
400	8040	515	181
500	8001	527	208
600	7962	558	223
700	7925	568	248
800	7884	680	261
900	7845	640	321
1000	7806	620	308
1100	7767	640	318
1170	7727	650	337
1336	7400	720	349
1400	7340	723	353
1500	7250	740	353
1600	7160	764	353

Table 3 Temperature-dependent friction coefficient values of Inconel 718

SL No.	Temperature, °C	Friction coefficient
1	25	0.30
2	300	0.25
3	420	0.20
4	543	0.01

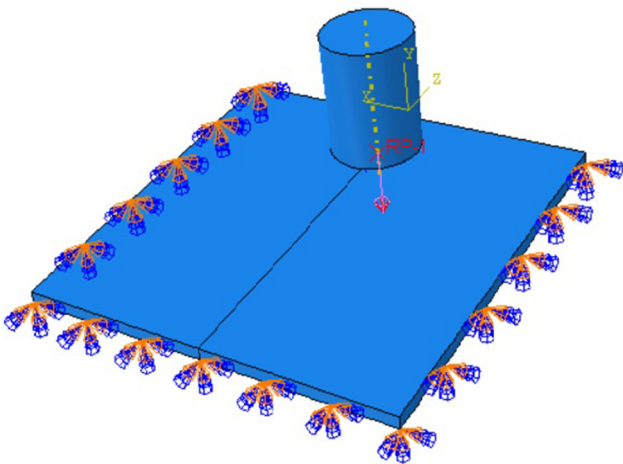


Fig. 6 Boundary conditions and axial load

the welding seam. The tool rotational speed and transverse speed of 300 rpm and 90 mm/min have been used to simulate the FE model in this work in order to investigate the reason behind the improvement in mechanical properties during experimental work. In the present model, a plunge time of 1.0 s is considered. The dwell time is of 2.0 s, and the tool traverse period of 7.0 s is considered. Nlgeom was kept on in order to account for the nonlinearity in geometry evolving out of large temperature generations and high deformations during the friction stir welding process.

3.4 Governing Equations

The heat generation in the process occurs due to friction between the tool and the workpiece and secondly due to plastic deformation in the nugget zone. Heat dissipation occurs through conduction from tool to the workpiece and also by the other modes of transfer from the open surfaces. However, radiation heat transfer is negligible due to low temperatures. The heat transfer phenomenon is governed by the following equation in Cartesian coordinates,

$$\rho C_p \frac{\partial T}{\partial t} = \frac{\partial}{\partial x} \left[k_x \frac{\partial T}{\partial x} \right] + \frac{\partial}{\partial y} \left[k_y \frac{\partial T}{\partial y} \right] + \frac{\partial T}{\partial z} \left[k_z \frac{\partial T}{\partial z} \right] \quad (\text{Eq 2})$$

where ρ and C_p are density and specific heat, respectively, k_x , k_y and k_z are heat conductivities in three directions, T is temperature, and t is time.

Conventional Coulomb friction law is generally followed in the contact property in friction stir welding methods. The following equation describes the shear stress generated on the contact surface:

$$\tau = \mu P \quad (\text{Eq 3})$$

where τ is the frictional shear stress, μ is the coefficient of friction, and P is the normal pressure. Therefore, the heat generation from the friction is described as follows:

$$q = \eta \dot{\gamma} \tau = \eta \mu P \dot{\gamma} \quad (\text{Eq 4})$$

where $\dot{\gamma}$ is called slipping rate and η is the heat conversion efficiency. However, Coulomb friction law is applicable only in the initial phase for relatively low temperatures. As the process proceeds, high temperatures are developed and friction follows a viscoelastic behavior. A modified Coulomb friction law is then used to define the heat generation given by the following equation:

$$q = \eta \dot{\gamma} \min(\mu P, \sigma/\sqrt{3}) \quad (\text{Eq 5})$$

where σ is the flow stress of the material.

Furthermore, the mechanical response is controlled by ABAQUS following the suggestion of Li et al. (Ref 18) as follows:

$$\rho a = \rho g + \text{div}(\sigma) \quad (\text{Eq 6})$$

where g is the body force per unit mass, ρ is the mass density, σ is the stress tensor, and a is the acceleration. ABAQUS/Explicit platform applies the central difference rule as suggested by Luo et al. (Ref 19) to solve the mechanical response equation.

The following assumption has been made for simplification of the model:

- Heat loss due to radiation is negligible.
- Gravity does not affect the welding process.
- No tilt angle is given to the spindle of the tool.
- Heat generation inside the material is considered as negligible.
- Heat loss from workpiece to tool is neglected.

4. Model Results and Discussion

This section discusses the results obtained from the numerical simulations using the above presented ALE model. Tool rotation speed was set at 300 rpm, and traverse speed was fixed at 90 mm/min.

4.1 Temperature Distribution

The finite element model developed in this work holds the ability to analyze the significant FSW outcomes like temperature distribution, stress distribution, plunge pressure, etc., throughout the entire process for Inconel 718. ABAQUS/EXPLICIT software is used to perform the thermomechanical analysis during the three steps namely plunging, dwelling and traverse stages.

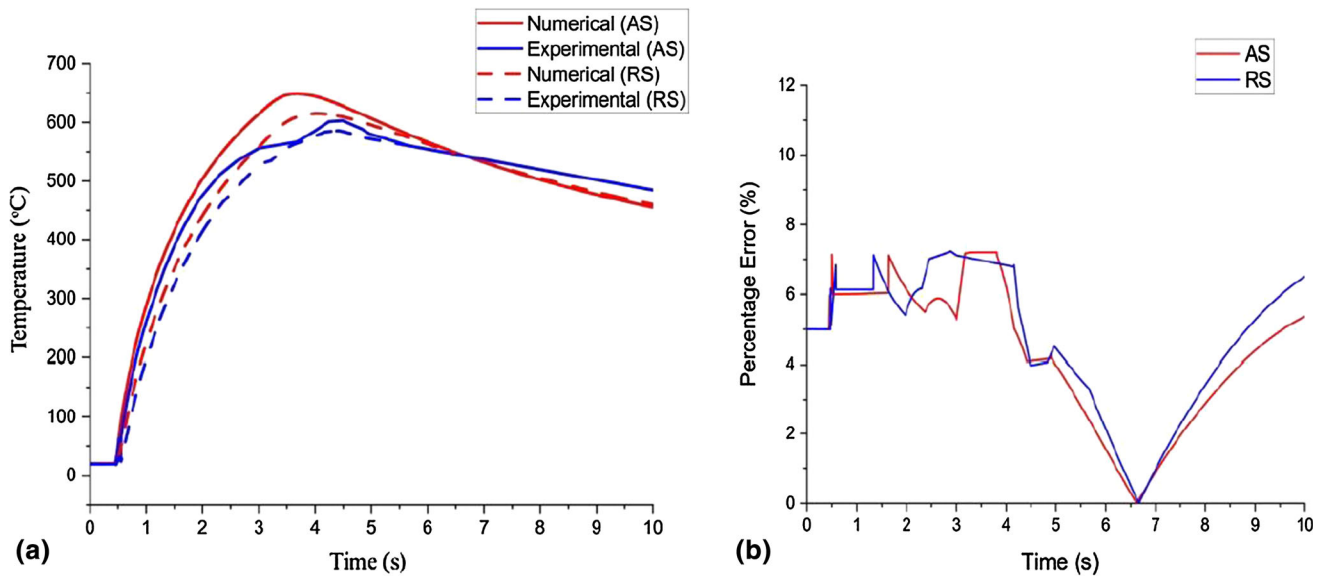


Fig. 7 (a) Comparison of experimental and numerical thermal profiles for welds and (b) error curves representing percentage error between experimental and numerically obtained thermal profiles in the advancing side (AS) and retreating side (RS)

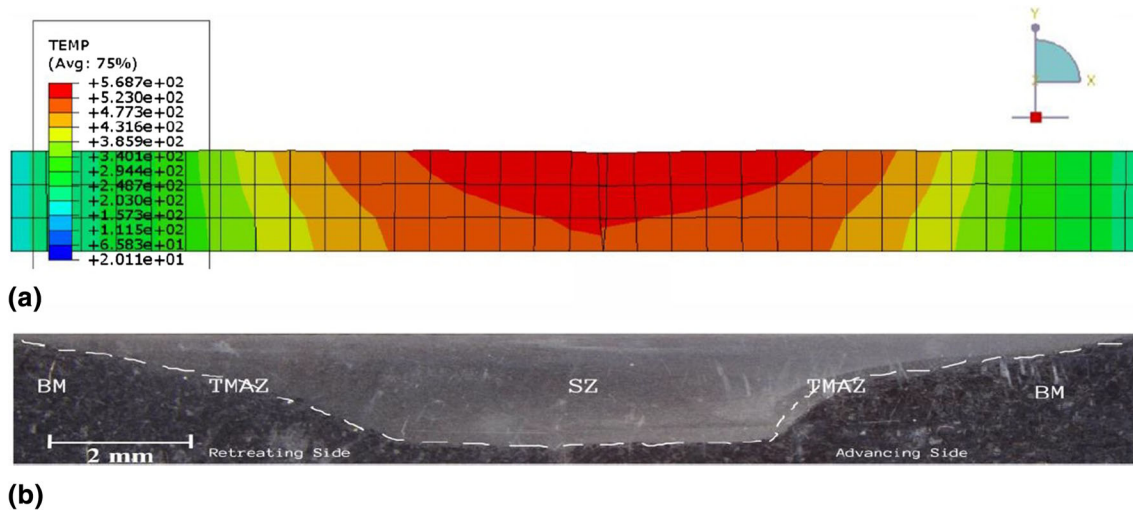


Fig. 8 Comparison of cross-sectional view for welds obtained: (a) numerical result (b) experimental work, showing temperature contours at a point during traverse stage

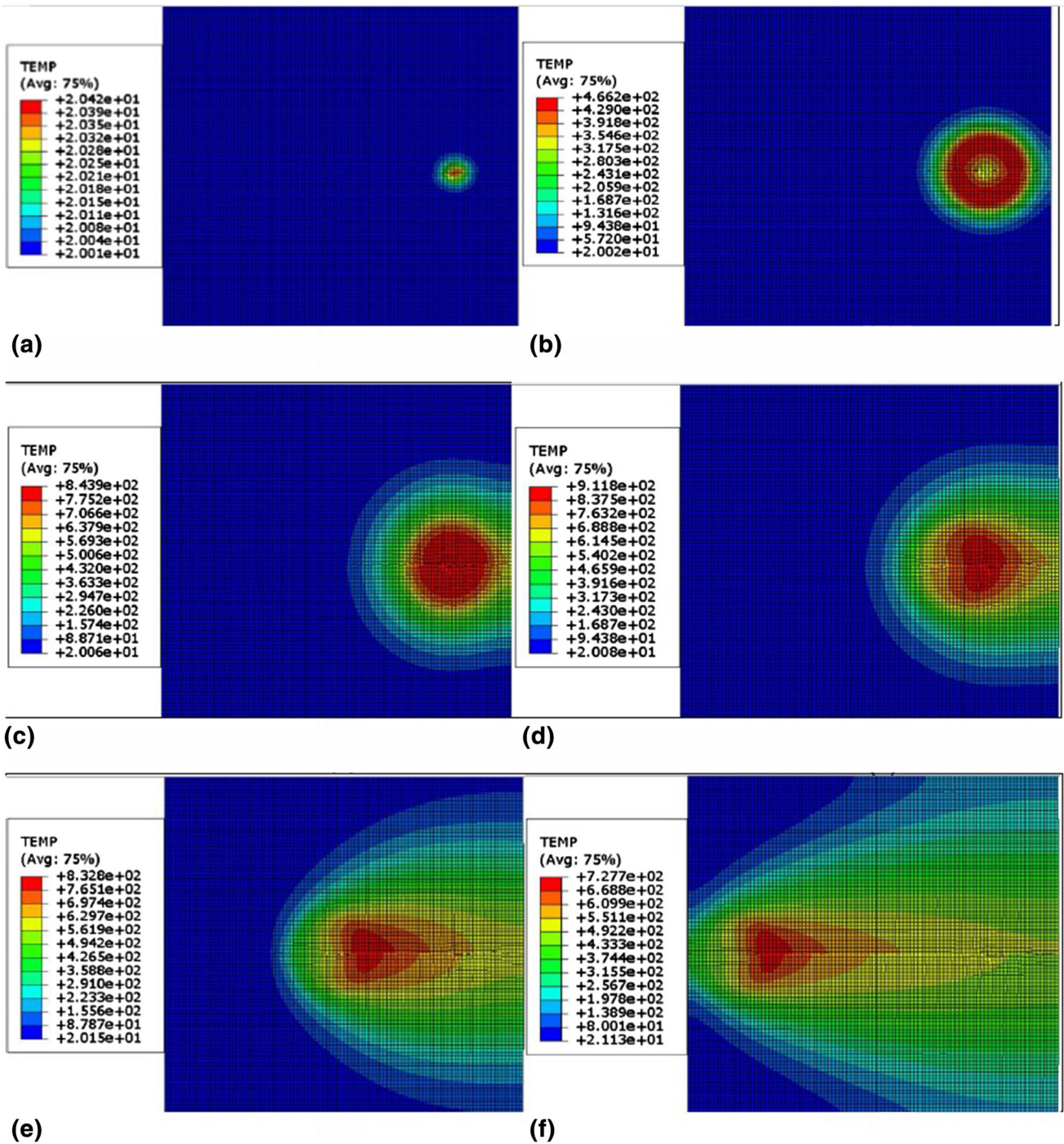


Fig. 9 Temperature distribution along the weld line: (a) beginning of plunge (0.39 s); (b) end of plunge (1.0 s); (c) end of dwell (3.0 s); (d) beginning of traverse (4.043 s); (e) mid-traverse (6.577 s) and (f) end of welding (10.0 s)

Figure 7(a) demonstrates the thermal profiles generated during experiment and numerical analyses. The numerical results obtained were similar to the previously obtained experimental results. However, the numerical results overestimated the temperature data by a margin of 7 % (Fig. 7b). Similar results were obtained in the literature (Ref 5, 7). This could be due to the approximation of the convective heat transfer coefficients, negligence of radiation heat losses and overlooking the heat transfer from workpiece to the tool during stirring action. Furthermore, temperature on the advancing side

was slightly higher than that of the retreating side. The reason behind this difference may be that on the advancing side, the stirring action of the tool is only utilized in frictional heat generation, while on the retreating side, the stirring action is accompanied by pushing the material ahead of the tool. Figure 8 shows the transverse and longitudinal cross-sectional view of the joined plates during welding process.

It is evident that the numerically obtained cross section shows excellent correlation to the experimentally obtained cross section of the weld. Highest temperature is achieved in

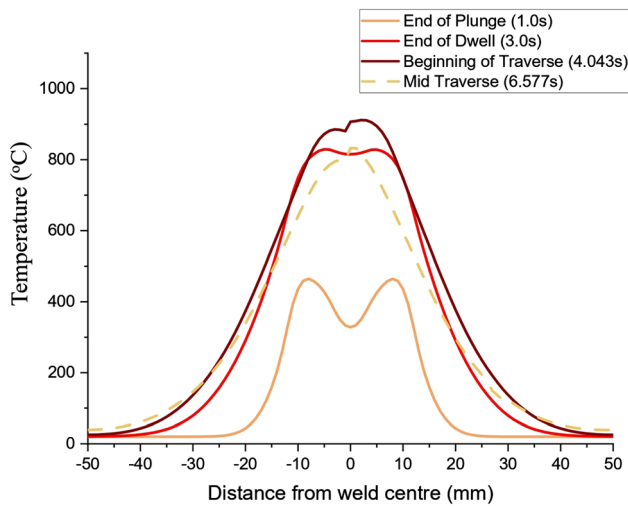


Fig.10 Temperature vs distance across the weld line calculated from simulation results

the SZ. The temperature distribution along the weld line at various time points is shown in Fig. 9 corresponding to the plunge, dwell and traverse stage. A 10-second process period was used to demonstrate the plunge (1 s), dwell (2 s) and traverse stage (7 s). Contour plots indicate that maximum temperature during plunge stage (Fig. 9a) is generated in the zone where pin touch the plate surface (indicated in red) heat transfers evenly in all directions through a semi-circular contour. Temperature then continues rising at high rates until the pin is completely inserted into the plate thickness and shoulder comes in complete contact with the plate surface.

Maximum temperature is generated in the corner area formed by plate and shoulder bottom surface (Fig. 9b) (Ref 4). The plunge forces and torques are also expected to be highest during the plunge stage. In the dwell period, stirring process softens the metal and rate of rise in both temperature and axial force decreases. After 3.0 seconds, i.e., at the end of the dwell period, the temperature reaches a maximum value of 843.9 °C. Temperature rise occurs until the beginning of the third stage, heading to a maximum of 911.8 °C at a process time of 4.043 seconds (Fig. 9d). This may be due to the complete contact between tool and workpiece. Hereon, the temperature profile remains more stable. Figure 10 shows the variation of temperature across the weld line at different process periods. It is evident that the temperature curve follows a symmetrical profile in both the advancing side (AS) and retreating side (RS), indicating that the direction of tool rotation has minimal impact on the thermal profiles of AS and RS. Therefore, this follows the previous investigations in the literature (Ref 18, 7). It is worthy to note that the highest temperature generated in case of conventional FSW is about 70 % of the melting point of Inconel 718 (Fig. 10). The maximum temperature achieved is well below the melting point of Inconel 718 alloy. This makes the present finite element model a potential tool in numerical analysis of FSW for accurate results.

4.2 Residual Stress Distribution

The ALE finite element model developed in this work was explored to study the stresses generated in the workpieces during the welding process. Figure 11 demonstrates the von Mises stress

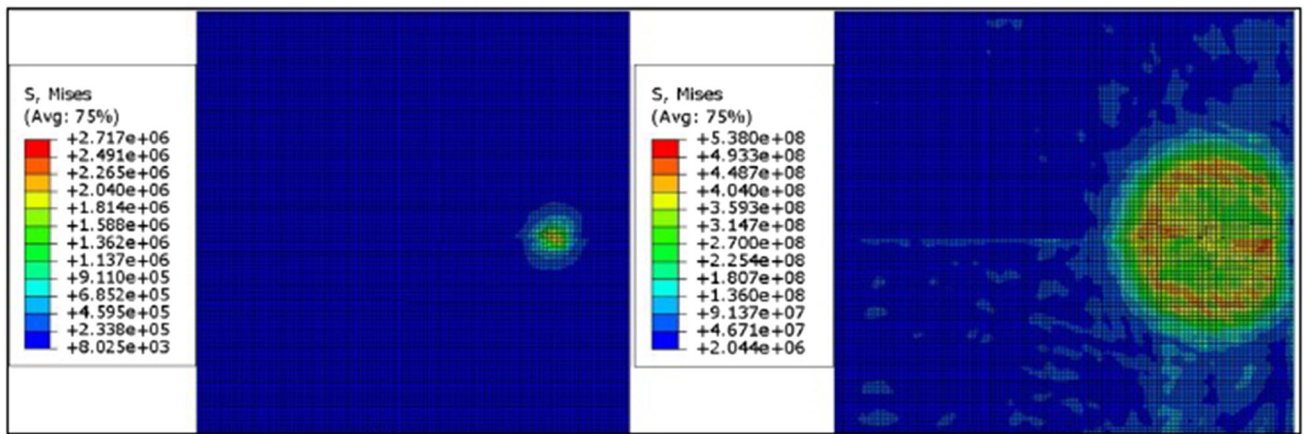
contours developed in the Inconel plates during FSW process at six different time locations spread over the three stages. As is evident from Fig. 11(a), initially, stresses were generated right beneath the tool pin and the surrounding area. As the pin penetrates more and more into the plate, high compressive stresses are created primarily because of the axial load application (Fig. 11b). As the contact between tool and workpiece material increases, temperature increases and hence material softening triggered by stirring action leads to reduction in resistance to material flow. Hence, motion of tool becomes easy leading to reduction in stresses locally as shown in Fig. 11(c) and (d). High stress contours move away from the pin-plate interface. Stresses further reduce during dwell period and early traverse phase, where highest temperature was generated, reaching 468 MPa in the circumference of shoulder and 313 MPa in the stir zone. Also, high stress contours slide away from the pin workpiece interface region with increasing temperature and surround the circumference of the shoulder. After 4.043 seconds, not much variation of stresses occurs in and around the stir zone. However, few scattered high stress regions develop away from the tool workpiece interface region as shown in Fig. 11(e) and (f). Stresses in these regions rise up to 739 MPa. This could be due to the dimensional constraints used in the model. Figure 12 further supports the above discussion through graphical representation of the variation of Mises stress across the weld plates at various time intervals.

Figure 12 clearly reveals that the maximum stress regions accumulate at the corner areas between shoulder bottom surface and plate top surface. Lowest stress values are observed in the beginning of the traverse phase where maximum temperatures are reached. Similar stress profiles were obtained in the work of Riahi and Nazari (Ref 17). Therefore, the FE model developed in this work proposes excellent candidature toward predicting the stress contours in FSW process. Furthermore, it can be concluded that the temperature profiles play an important role in controlling stress magnitude and hence yielding sound welds. This conclusion is in accordance with the work of Salloomi et al. (Ref 7).

5. Conclusions

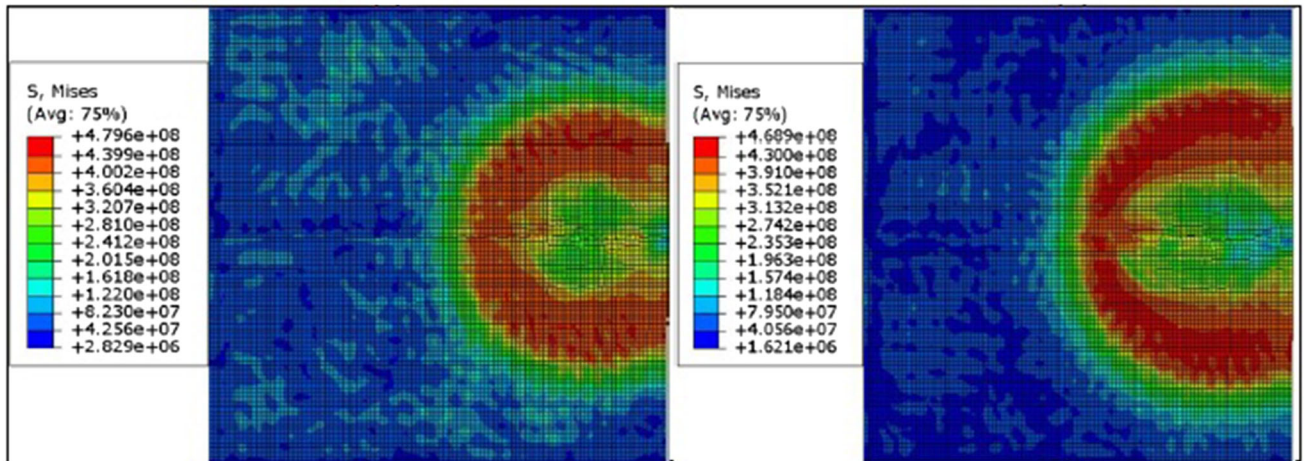
In this study, a 3D explicit finite element analysis was done in ABAQUS software package to predict the temperature distribution and coupled stress generated during friction stir welded Inconel 718 alloy. The numerical results were also validated through experimental results. From the above experimental and numerical investigations, the following conclusions can be drawn:

- The numerical and experimental thermal history was successfully validated with a maximum error of 7% in the maximum temperature. Hence, it can be concluded that the current FE model can be utilized in real-time applications for predicting the thermal history of Inconel alloys.
- At 90 mm/min of traverse speed, maximum temperature reached in FSW was 911.8 °C, which is well below the melting point temperature of Inconel 718, hence indicating a solid-state welding process.
- Analysis of mechanical response revealed reduction in stress magnitudes with increasing temperature. Also, high-stress regions slide away to the corners between the plate-shoulder interface.



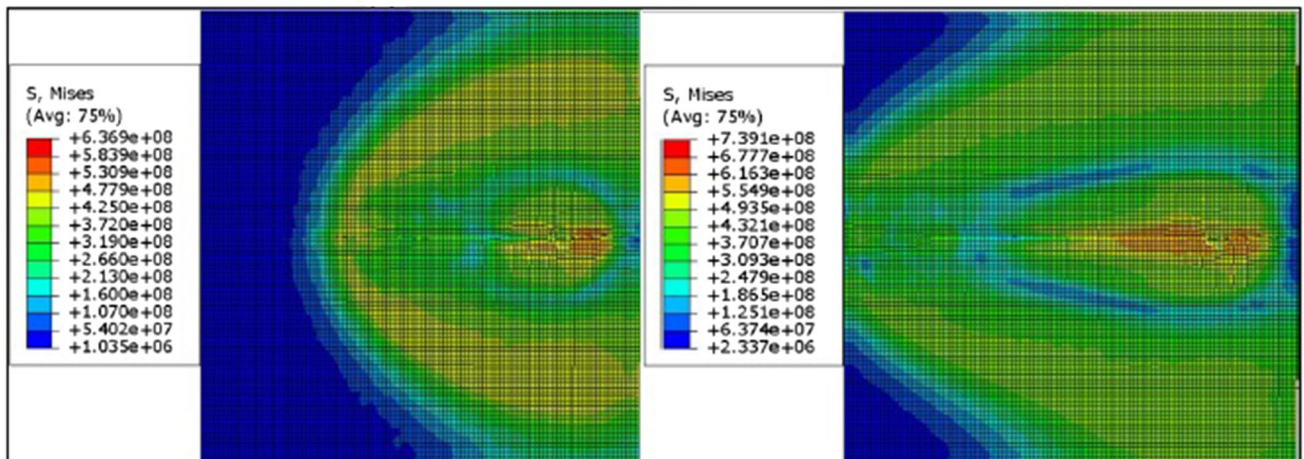
(a)

(b)



(c)

(d)



(e)

(f)

Fig. 11 Distribution of von Mises stresses developed in the plates: (a) beginning of plunge (0.39 s); (b) end of plunge (1.0 s); (c) end of dwell (3.0 s); (d) beginning of traverse (4.043 s); (e) mid-traverse (6.577 s) and (f) end of welding (10.0 s)

- Stress profiles showed significant correlation to the thermal profiles. Hence, it was concluded that the temperature profiles play a significant role in controlling stress magnitudes, hence yielding sound welds.
- As Inconel 718 alloy is a high-strength and high-melting-point alloy, so FSW of required very high plunging force and torque. High temperature, high plunging force and torque have a significant effect on the FSW tool degrada-

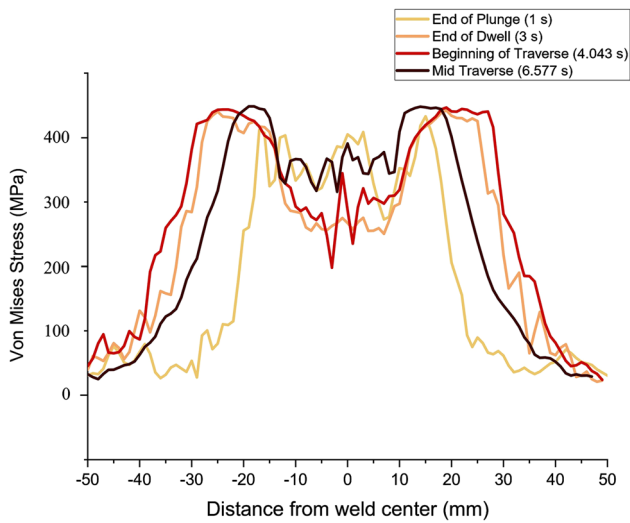


Fig.12 Von Mises stress vs distance across the weld line calculated from simulation results

tion. So, this means an additional preheat source can be used as an improvement of the conventional FSW process. Also, the finite element model can be used to develop different tool designs with an aim to improve the material flow and hence bond quality.

Conflict of interest

No potential conflict of interest was reported by the author.

References

- Z.Y. Ma, A.H. Feng, D.L. Chen and J. Shen, Recent Advances in Friction Stir Welding/Processing of Aluminum Alloys: Microstructural Evolution and Mechanical Properties, *Crit. Rev. Solid State Mater. Sci.*, 2017, **43**, p 1–65
- G. Çam, Friction Stir Welded Structural Materials: Beyond Al-Alloys, *Int. Mater. Rev.*, 2011, **56**, p 1–48
- C.M. Chen and R. Kovacevic, Finite Element Modeling of Friction Stir Welding—Thermal and Thermomechanical Analysis, *Int. J. Mach. Tools Manuf.*, 2003, **43**, p 1319–1326
- M. Yu, W. Li, J. Li and Y. Chao, Modelling of Entire Friction Stir Welding Process by Explicit Finite Element Method, *Mater. Sci. Technol.*, 2012, **28**, p 812–817
- K. Kumar, Numerical Simulation of Friction Stir Butt Welding Processes For Az91 Magnesium Alloy, *Int. J. Res. Eng. Technol.*, 2014, **03**, p 101–109
- P. Pankaj, P.S. Sawarkar, A. Tiwari, P. Biswas and S. Pal, Three Dimensional Fe Thermal Analysis for Friction Stir Welding of Low Carbon Steel, *Mater. Today: Proc.*, 2021, **41**, p 902–907
- K.N. Salloomi, F.I. Hussein and S.N.M. Al-Sumaidae, Temperature and Stress Evaluation during Three Different Phases of Friction Stir Welding of AA 7075-T651 Alloy, *Modell. Simul. Eng.*, 2020, **2020**, p 1–11
- Z. Zhang, J.T. Chen, Z.W. Zhang and H.W. Zhang, Coupled Thermo-Mechanical Model Based Comparison of Friction Stir Welding Processes of AA2024-T3 in Different Thicknesses, *J. Mater. Sci.*, 2011, **46**, p 5815–5821
- M. Assidi, L. Fourment, S. Guerdoux and T. Nelson, Friction Model For Friction Stir Welding Process Simulation: Calibrations From Welding Experiments, *Int. J. Mach. Tools Manuf.*, 2010, **50**, p 143–55
- R. Jain, S.K. Pal and S.B. Singh, A Study on the Variation of Forces and Temperature in a Friction Stir Welding Process: A Finite Element Approach, *J. Manuf. Process.*, 2016, **23**(23), p 278–286
- Y.J. Chao, X. Qi and W. Tang, Heat Transfer in Friction Stir Welding—Experimental and Numerical Studies, *J. Manuf. Sci. Eng.*, 2003, **125**, p 138–145
- H. Schmidt, J. Hattel and J. Wert, A Local Model For The Thermomechanical Conditions in Friction Stir Welding, *Modell. Simul. Mater. Sci. Eng.*, 2005, **13**, p 77–93
- S. Mandal, J. Rice and A.A. Elmustafa, Experimental and Numerical Investigation of the Plunge Stage In Friction Stir Welding, *J. Mater. Process. Technol.*, 2008, **203**, p 411–419
- W.Y. Li, M. Yu, J.L. Li and D.L. Gao, Explicit Finite Element Analysis of the Plunge Stage of Tool in Friction Stir Welding, *Mater. Sci. Forum*, 2009, **620–622**, p 233–236
- E. Uhlmann, M. Graf von der Schulenburg and R. Zettler, Finite Element Modeling and Cutting Simulation of Inconel 718, *CIRP Annals*, 2007, **56**, p 61–64
- F. Al-Badour, N. Merah, A. Shuaib and A. Bazoune, Thermo-Mechanical Finite Element Model of Friction Stir Welding of Dissimilar Alloys, *Int. J. Adv. Manuf. Technol.*, 2014, **72**, p 607–617
- M. Riahi and H. Nazari, Analysis of Transient Temperature and Residual Thermal Stresses in Friction Stir Welding of Aluminum Alloy 6061-T6 via Numerical Simulation, *Int. J. Adv. Manuf. Technol.*, 2011, **55**, p 143–152
- H. Li, D. Mackenzie and R. Hamilton, Multi-Physics Simulation of Friction Stir Welding Process, *Eng Comput*, 2010, **27**, p 967–985
- H. Luo, L. Xiao, J. Wu, H. Zhang and W. Zhou, Structure Design and Thermal Analysis of a New Type of Friction Stir Weld Spindle, *Adv Mech Eng*, 2017 <https://doi.org/10.1177/1687814017700060>
- I. Hernando, M.A. Renderos, M. Cortina, J. Exequiel Ruiz, J.I. Arrizubieta and A. Lamikiz, Inconel 718 Laser Welding Simulation Tool Based on a Moving Heat Source and Phase Change, *Procedia CIRP*, 2018, **74**, p 674–678
- C.A. Hernández, V.H. Ferrer and J.E. Mancilla, Three-Dimensional Numerical Modeling of the Friction Stir Welding of Dissimilar Steels, *Int. J. Adv. Manuf. Technol.*, 2017, **93**, p 1567–1581
- X.K. Zhu and Y.J. Chao, Numerical Simulation of Transient Temperature and Residual Stresses in Friction Stir Welding of 304L Stainless Steel, *J. Mater. Process. Technol.*, 2004, **146**, p 263–272
- R. Nandan, G.G. Roy, T.J. Lienert and T. DebRoy, Numerical Modelling of 3D Plastic Flow and Heat Transfer During Friction Stir Welding of Stainless Steel, *Sci. Technol. Weld. Join.*, 2006, **11**, p 526–537

Publisher's Note Springer Nature remains neutral with regard to jurisdictional claims in published maps and institutional affiliations.